Article

H-ZSM-5 Materials Embedded in an Amorphous Silica Matrix: Highly Selective Catalysts for Propylene in Methanol-to-Olefin Process

Huda Sharbini Kamaluddin[ID]**, Sulaiman Nassir Basahel, Katabathini Narasimharao * and Mohamed Mokhtar ***[ID]

Surface Chemistry and Catalytic Studies (SCCS) Group, Department of Chemistry, King AbdulAziz University, Jeddah 21589, Saudi Arabia; hudashkamaluddin@gmail.com (H.S.K.); sbasahel@hotmail.com (S.N.B.)

* Correspondence: nkatabathini@kau.edu.sa (K.N.); mmoustafa@kau.edu.sa (M.M.);
  Tel.: +96-65-3863-8994 (K.N.); +96-65-0055-8045 (M.M.)

check for updates

Abstract: H-ZSM-5 materials embedded in an amorphous silica were successfully synthesized with three different Si/Al ratios (i.e., 40, 45, and 50). The presence of the MFI structure in the synthesized samples was confirmed by X-ray diffraction (XRD), Fourier transform infra-red (FT-IR), and solid state-nuclear magnetic resonance (SSNMR) techniques. The morphology and textural properties of the samples were investigated by scanning electron microscopy (SEM), TEM, and N_2-physisorption measurements. Furthermore, acidic properties of the synthesized catalysts have been studied by NH_3-TPD and FT-IR spectroscopy of CO adsorption studies. Variation of the Si/Al ratio affected the crystal morphology, porosity, and particle size, as well as the strength and distribution of acid sites. The synthesized zeolite materials possessed low acid-site density and exhibited high catalytic activity in the methanol-to-olefin (MTO) reaction. To study the intermediate species responsible for catalyst deactivation, the MTO reaction was carried out at high temperature (500 °C) to accelerate catalyst deactivation. Interestingly, the synthesized catalysts offered high selectivity towards the formation of propylene ($C_{3=}$), in comparison to a commercial microporous crystalline H-ZSM-5 with Si/Al = 40, under the same reaction conditions. The synthesized H-ZSM-5 materials offered a selectivity ratio of $C_{3=}/C_{2=}$ 12, while it is around 2 for the commercial H-ZSM-5 sample. The formation of hydrocarbon species during MTO reaction over zeolite samples has been systematically studied with operando UV-vis spectroscopy and online gas chromatography. It is proposed that the strength and type of acid sites of catalyst play a role in propylene selectivity as well as the fast growing of active intermediate species. The effective conversion of methanol into propylene in the case of synthesized H-ZSM-5 materials was observed due to possession of weak acid sites. This effect is more pronounced in H-ZSM-5 sample with a Si/Al ratio of 45.

Keywords: mesoporous H-ZSM-5; methanol-to-olefin (MTO); propylene; acid sites density; operando UV-vis spectroscopy

1. Introduction

Propylene is one of the most important base chemicals in chemical industries. Due to the high demand for propylene, the development of more selective catalysts for the methanol-to-olefin (MTO) process is highly desired [1,2]. So far, crystalline zeolite and zeolite-like materials have been the most studied catalysts in the MTO reaction, due to their unique physico-chemical properties, including acidity, topology, and shape selectivity [3–5] Usually, zeolites with 8- to 10-membered rings, such as H-SAPO-34 (CHA) and H-ZSM-5 (MFI), have been used as selective and stable catalysts for the MTO

process [6,7]. Therefore, many researchers have explored different strategies to synthesize zeolites with different structures (particularly MFI and CHA) to improve propylene selectivity. The zeolite topology, e.g., structure, 1-, 2-, 3-dimention, shape, cage size, and channel system, affect the nature of the retained hydrocarbon pool that formed during MTO reaction, and, accordingly, the olefin product selectivity [8,9]. In addition to the effort of forming high selectivity towards propylene, Palčić et al. [10] studied the effect of crystallization temperature (170, 150, 120, and 100 °C) on the ZSM-5 properties. They observed that the decrease in the crystallization temperature 100 °C led to significant changes in zeolite properties exhibiting many framework defects with decrease in acid-site density, decrease in their strength, and larger external surface area. Those properties affected to the product selectivity in MTO reaction, and show a $C_{3=}/C_{2=} = 6$ with high selectivity towards propylene (53%). Moreover, Losch et al. [11] studied the effect of external surface passivation of ZSM-5 by chemical liquid deposition on its C_2-C_3 selectivity. A 10–30% increase in the C_2-C_3 selectivity was recorded for the passivated zeolites.

The MTO process is known to be greatly influenced by the Brønsted acid sites presented in the solid catalyst. The Brønsted and Lewis acid sites exist in the zeolites due to presence of tetrahedral framework Al atoms and/or silanol (Si–OH) groups within framework and extra-framework Al species [12]. It was suggested that existence of Brønsted and Lewis acid sites could lead to synergistic effects between the two types of acid sites [13]. Corma et al. [14] and Mirodatos et al. [13] proposed the mechanism of synergistic effect between two types of acid sites; the authors indicated that the extra-framework Al species directly interact with the acidic –OH groups, which involves partial electron transfer from O–H groups to the oxoaluminum species (AlO^+ and $AlOOH$). The electron transfer lead to delocalization of electron density around the O-atom, which is very similar to the super-acid systems ($AlCl_3$-HCl and SbF_5-HF).

It has also been reported that reactions of hydrocarbons over the strong Brønsted acid sites located on the outer surface of zeolite particles cause external coke deposition, leading to a short lifetime of catalysts [15]. Many efforts have already been reported to nullify the adverse effects of acid sites by minimizing the inner density of acid sites within the structure to prevent non-selective catalytic activity in the MTO process. Hadi et al. [16] used ion exchange procedure to exchange some acidic H^+ ions in the framework with Ca, Mn, Cr, Fe, Ni, Ag, and Ce ions. Some other strategies, such as changing the medium of zeolite preparation (fluoride route) [17], altering Si/Al ratio, synthesizing distorted zeolite framework, building hierarchical zeolite materials [1,18,19], preparing composite molecular sieves [20,21], and synthesizing the nanosheet framework to decrease long channels [22], were employed. In addition, several research groups focused on tuning the reaction conditions, e.g., increasing the reaction temperature, decreasing the partial pressure of methanol, changing the reactor design [23], and introducing a co-feed of methanol containing water to the MTO reaction [24]. Consequently, selectivity towards light olefins can be increased by decreasing the selectivity towards aromatic products [25]. Yarulina et al. [26] incorporated Ca into ZSM-5 structure and observed an increase of propylene selectivity. The authors claimed that modification with Ca^{2+} resulted in a decrease in the acidity of the zeolite. As a result, the rate of hydride transfer and oligomerization reactions on these sites is greatly reduced, causing the suppression of ethylene selectivity. In another report, Yarulina et al. [27] also studied the effect of acidity on the catalytic activity of the ZSM-5 for the MTO process; the authors observed that the introduction of Lewis acid sites averts coke formation, thus enhancing the lifetime of the catalyst and also observing that the isolation of Brønsted acid sites is essential to increase propylene selectivity.

Several decades ago, Jacobs et al. [28] reported the existence of X-ray amorphous ZSM-5 material, which contained zeolite particles of less than 8 nm sizes embedded in an amorphous matrix of silica. Later, Nicolaides [29] reported the synthesis of substantially amorphous ZSM-5 materials at various temperatures under autogenous pressure. Triantafyllidis et al. [30] reported the hydrothermal synthesis of X-ray amorphous samples at temperature as low as 25 °C. The authors observed that the materials consisted of well-formed particles of almost spherical shape and with dimensions of about 20–30 nm. Corma and Daiz-Caban [31] also synthesized amorphous zeolite materials using the

self-assembly of organic structure-directing agents. Significant efforts have been made to synthesize ZSM-5 materials embedded in amorphous silica without using any seeding agent [32]. Kim and Kim [33] successfully synthesized ZSM-5 materials in the absence of template or seeding agent using two-step temperature technique. Recently, a modified method for the synthesis of an amorphous ZSM-5 has been reported by Yeong et al. [34]. Our group also synthesized ZSM-5 materials containing amorphous silica matrix using aluminum nitrate as Al source for the first time without using any organic template [35]. Many research groups have reported on the synthesis and characterization of ZSM-5 materials embedded in amorphous silica, but these materials were not explored for catalytic application in the MTO process [36].

In this research, H-ZSM-5 materials with different Si/Al ratios (40, 45, and 50) embedded in amorphous silica were synthesized; the acid-site density of the H-ZSM-5 materials decreased by intercepting the crystallization process and making use of a unified crystallization time of 16 h. The physico-chemical properties were studied by different methods and the materials were used as catalysts in the MTO process. It is also our aim to understand the intermediate species responsible for catalyst deactivation in the MTO process at high temperature; therefore, the catalytic performance of the synthesized materials was studied at 500 °C. Furthermore, we used a combination of operando UV-vis spectroscopy and online gas chromatography to correlate and elucidate the catalytic activity with the formation of different active and deactivating hydrocarbon species generated in the catalyst bed.

2. Results and Discussion

2.1. Structure, Morphology, and Porosity of Synthesized Materials

Figure 1 shows powder X-ray diffraction (XRD) patterns of the H-ZSM-5 materials embedded in amorphous silica along with a commercial Zeolyst sample. The synthesized materials exhibited major reflections in the ranges of 2θ = 8–11° and 27–30° corresponding to the MFI structure [ICDD file no. 41–1478]. The XRD patterns also show additional broad humps corresponding to silica, indicating that the synthesized samples are composed of both ZSM-5 and silica phases. It is clear from Figure 1 that the intensity of the reflections of the MFI-40 sample is higher than those of the MFI-45 and MFI-50 samples. This observation indicates that the Si/Al ratio of the synthesized materials has an influence on the crystal size of ZSM-5 structure; crystallite increased with the increase of Si/Al ratio (Table 1).
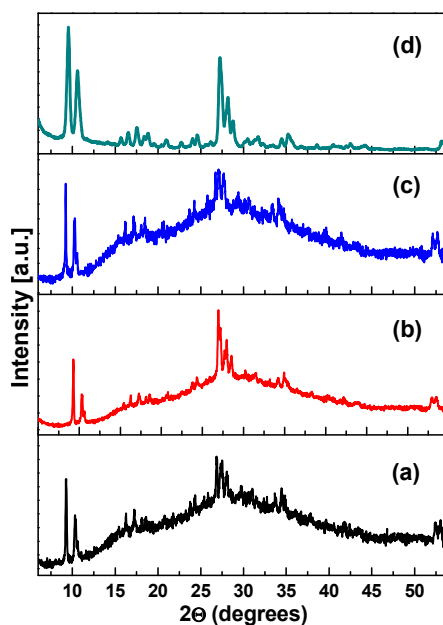

Figure 1. Powder X-ray diffraction (XRD) patterns of the synthesized samples; (**a**) MFI-40, (**b**) MFI-45, (**c**) MFI-50, and (**d**) Zeolyst.

Table 1. Crystallite size, chemical composition, and textural properties for synthesized H-ZSM-5 and Zeolyst samples.

Sample	Si/Al Ratio [a]	Average Crystal Size (nm) [b]	S_{BET} [c] (m²/g)	S_{micro} (m²/g)	S_{meso} (m²/g)	V_{Total} [d] (cm³/g)	V_{micro} [e] (cm³/g)	V_{meso} [f] (cm³/g)	Hierarchy Factor [g]
MFI-40	42	89	383	358	45	0.901	0.039	0.862	0.005
MFI-45	46	126	403	322	81	1.141	0.042	1.099	0.007
MFI-50	53	140	420	347	73	1.057	0.049	1.008	0.008
Zeolyst	40	63	262	115	147	0.115	0.098	0.017	0.478

[a] ICP-MS analysis; [b] estimated from XRD analysis; [c] Brunauer-Emmett-Teller (BET) surface area; [d] Total pore volume at $P/P_o = 0.997$; [e] Micropore volume from *t*-plot; [f] $V_{meso} = V_{Total} - V_{micro}$; [g] Hierarchy factor = $(V_{micro}/V_{Total}) \times (S_{meso}/S_{BET})$.

Fourier transform infra-red (FT-IR) spectral analysis was used to confirm the presence of the MFI structure in the synthesized samples, since Jacobs et al. [28] indicated that XRD should be used with caution for ZSM-5 materials embedded in an amorphous silica. The authors recommended the FT-IR technique to determine the MFI structure as the vibrations of the zeolite skeleton are intense even for agglomerates of a few unit cells. Figure S1 shows the FT-IR spectra of the synthesized materials along with Zeolyst ZSM-5 sample. A band at ~550 cm⁻¹ was observed in all the samples, which corresponds to the vibration of a five-membered ring (Pentasil) for the MFI structure [37]; however, the intensity of this band decreased with increasing Si/Al ratio. Furthermore, a broad band at around 1060 cm⁻¹ due to an internal vibration of (Si,Al) O_4 tetrahedron (T) of the MFI structure was also observed for the synthesized samples. These results clearly indicate the presence of MFI structure in synthesized H-ZSM-5 samples. FT-IR analysis was also used to study the characteristics of different hydroxyl groups presented in the MFI framework of the samples (Figure 2).
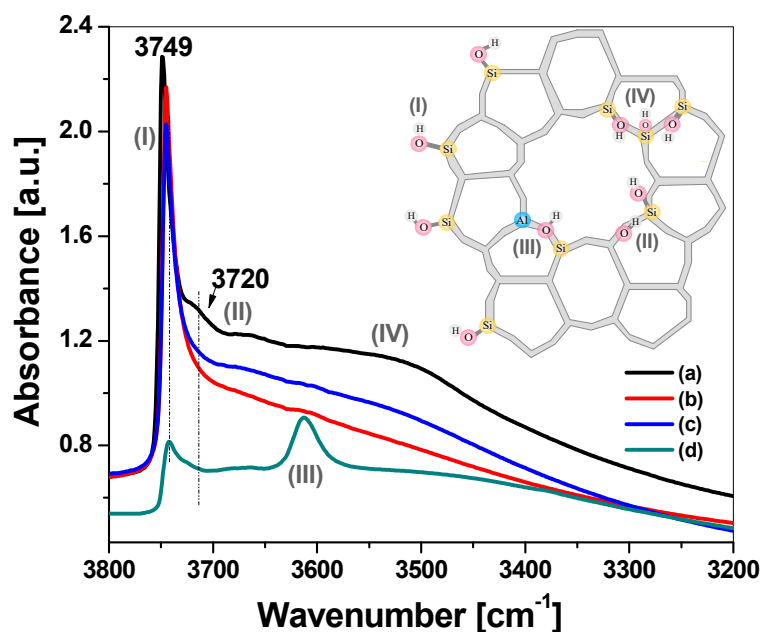
Figure 2. Fourier transform infra-red (FT-IR) spectra for studied materials (**a**) MFI-40; (**b**) MFI-45; (**c**) MFI-50 and (**d**) Zeolyst.

The analysis was performed after outgassing the samples at 300 °C under vacuum. The band at 3749 cm⁻¹ (I) corresponds to the external Si-OH groups and the intensity of this band is very low in the case of the Zeolyst compared to synthesized samples. It was proposed that appearance of the intense band at 3749 cm⁻¹ is an indication of the amorphous nature of the samples with low Al content that possessed high external surface area [17,38,39]. The IR band for terminal isolated Si-OH groups at 3720 cm⁻¹ (II) are clearly observed as a weak shoulder in the case of the Zeolyst and MFI-40 samples. The shoulder is very weak and broad in the Zeolyst compared with the MFI-40 sample. The intense IR

band at 3612 cm^{-1} (III) corresponding to the internal vibration of Brønsted acid sites [38], which is very sharp in Zeolyst sample compared to synthesized H-ZSM-5 samples, indicates the presence of high density of Brønsted acid sites in the Zeolyst sample. Interestingly, a broad envelope appeared centered at ~3500 cm^{-1} (IV) related to Si-OH nests that comprised many Si-OH groups interacting through extended H-bonding, and this type of nest generally forms at crystal steps or extended defects [38]. Among studied samples, the MFI-40 sample exhibited the broadest envelope.

The morphology of the synthesized samples was investigated using the scanning electron microscopy (SEM) technique. The SEM images of the samples are shown in Figure 3. The MFI-40 and MFI-45 samples contained crystalline MFI particles with a polygon shape surrunded by amorphous material. On the other hand, the MFI-50 sample possessed agglomerated particles with no definite shape along with a large amount of amorphous material. Interestingly, the large particles presented in MFI-45 and MFI-50 samples did not represent the normal shape (coffin-like) of ZSM-5 crystals due to modified synthesis conditions. The Zeolyst sample showed presence of very large crystalline particles several micrometers in length and width.
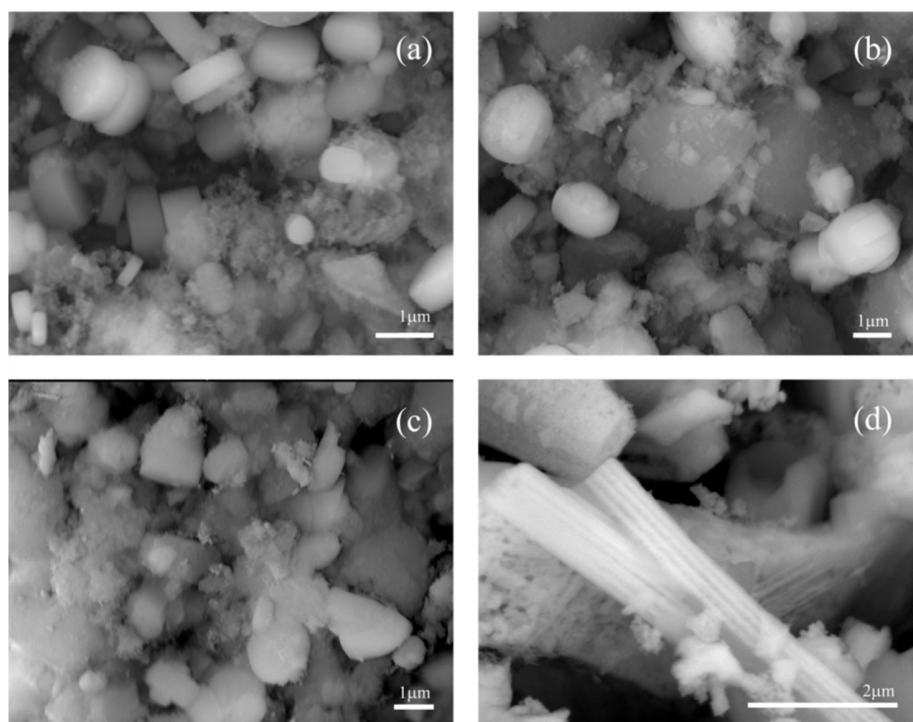
Figure 3. Scanning electron microscopy (SEM) images of the studied samples (**a**) MFI-40, (**b**) MFI-45, (**c**) MFI-50 and (**d**) Zeolyst.

The N$_2$ adsorption-desorption isotherms of synthesized H-ZSM-5 and commercial Zeolyst samples are shown in Figure 4A. The pore-size distribution patterns, which were derived from the adsorption branches using the Non-Local Density Functional Theory (NLDFT) method, are shown in Figure 4B. The Zeolyst sample shows mixed type I and type IV isotherms according to the classification of international union of pure and applied chemistry (IUPAC), with a distinct hysteresis loop at relative pressure range between P/P$_o$ = 0.4 and 0.95, with a sharp increase of N$_2$ uptake between P/P$_o$ = 0.95 and 1.0, which are the characteristics of materials with micro- and meso-pores. This is verified by the NLDFT pore-size distribution pattern of Zeolyst sample, where there is a sharp peak below 20 Å (micropores) and a minor hump in the mesoporous range.
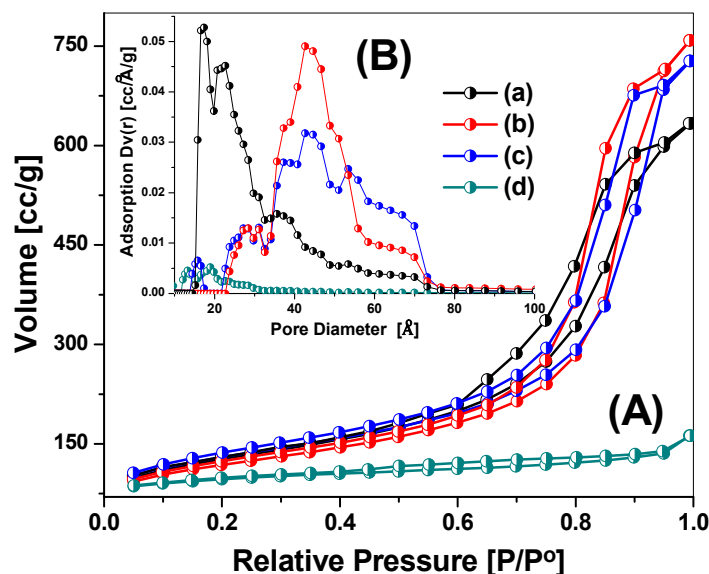
Figure 4. (**A**) N_2 adsorption-desorption isotherms and (**B**) pore-size distribution patterns of (**a**) MFI-40, (**b**) MFI-45, (**c**) MFI-50 and (**d**) Zeolyst.

The synthesized H-ZSM-5 (MFI-40, MFI-45 and MFI-50) samples showed type IV isotherms, with a hysteresis loop at relative pressures higher than $P/P_o = 0.4$, which is typical for mesoporous materials. These hysteresis loops are due to the capillary condensation in the mesopore void spaces [40]. The dramatic increase in the adsorption amounts at high relative pressure compared with isotherm of the commercial H-ZSM-5 sample is mainly due to the generation of mesopores due to voids in the three samples. Table 1 shows the Brunauer-Emmett-Teller (BET) surface area (S_{BET}), micropore surface area (S_{micro}), mesopore surface area (S_{meso}), total pore volume (V_{total}) micropore volume (V_{micro}), and mesopore volume (V_{meso}) of all the investigated samples. Their BET surface areas, total pore volumes, and mesopore volumes are higher than the commercial H-ZSM-5 sample (Table 1). The mesoporous volume for partially crystalline samples increases in the following order: MFI-40 < MFI-50 < MFI-45. The major difference between the synthesized H-ZSM-5 embedded in silica and Zeolyst sample is the presence of non-crystallographic intracrystalline mesopores resulting in the high porosity of synthesized zeolite compared to the conventional zeolite. Trintafyllidis et al. [30] indicated that the mesoporous nature could be due to the presence of some impurities, such as amorphous silica-alumina. It can be concluded that the sudden-stop of the crystallization process during synthesis to get mesoporous ZSM-5 is a very effective method.

To study the nature of Al and Si coordination sites, solid-state ^{27}Al and ^{29}Si MAS NMR spectra for the investigated samples were obtained. The ^{27}Al MAS NMR spectra for all the samples are shown in Figure 5A. The spectra exhibited two sharp NMR resonances centered at 56.1 ppm and 0 ppm corresponding to the Al^{IV} species presented in the framework of zeolite in a tetrahedral coordination [41] and Al^{VI} presented outside the zeolite framework in an octahedral coordination [42], respectively. The intensity of the resonance at 56.1 ppm for the synthesized ZSM-5 samples is low in comparison with the Zeolyst sample. This observation indicates that the incorporation of Al in the MFI framework is lower in synthesized samples compared to Zeolyst sample. The octahedral coordinated Al species, most probably existing in extra-framework position (EFAl$^+$), were dominant especially for the synthesized materials [43]. Deconvolution of the ^{29}Si MAS NMR spectra for all samples was performed in Figure 5B. All the samples showed a major resonance at −112 ppm; evidently a strong signal corresponding to Si(4Si) of Q_4 at high field side was shown in all high siliceous zeolites samples [44]. The other types of Si species such as Si attached to one, two, three, or four Al atoms through oxygens could be observed as shoulders [45]. In addition, the occurrence of a silanol group (Si-OH) led to a change in the coordination, Q_4, Q_3, Q_2 and chemical shift of about +10 ppm/OH [12]. The Zeolyst

sample showed only one small shoulder at −103.2 ppm, which could be assigned to Si(3Si,1Al) sites [41]. On the other hand, the synthesized samples showed two shoulders, the first one in the range of −103.2 ppm to −105 ppm, indicating the existence of Si atoms with chain and chain-branching structure Si(3Si,1Al) and Si(2Si,2Al), overlapped with Q_3 and Q_2 of Si-OH, respectively [46], and the second one in the range of −90. 2 ppm to −99 ppm, which is ascribed to AlOSi*(OSi)$_3$ and/or HOSi*(OSi)$_3$ of Q_3 signal [47]. Moreover, there are minute resonances recorded below −100 ppm, which correspond to Si(2Si,2Al) atoms indicating the presence of Al-O-Si-O-Al sequences in minor quantities in the synthesized samples [42].
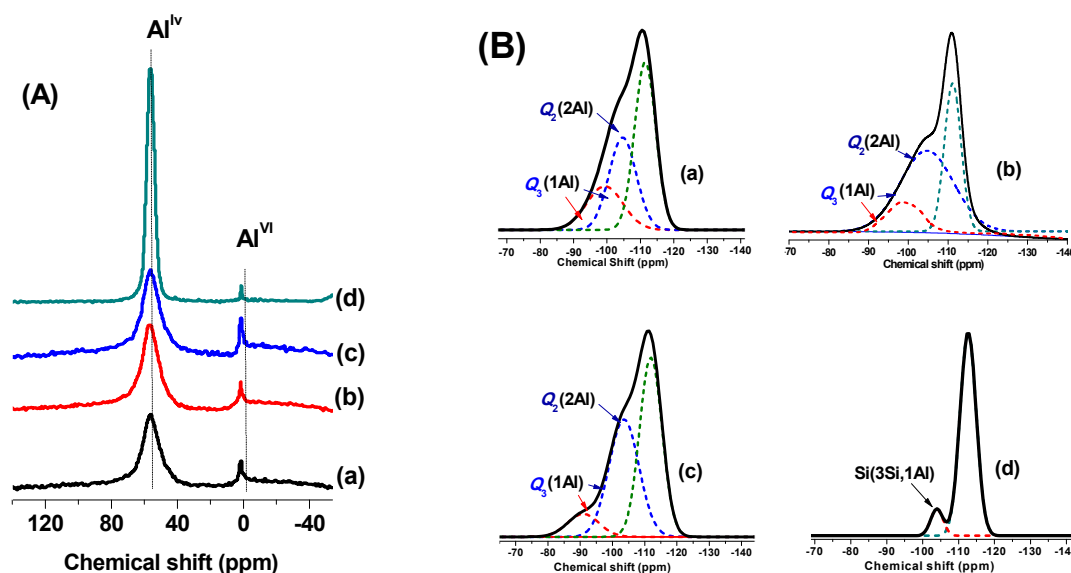
Figure 5. (**A**) ^{27}Al MAS NMR and (**B**) deconvoluted ^{29}Si MAS NMR of (**a**) MFI-40, (**b**) MFI-45, (**c**) MFI-50, and (**d**) Zeolyst samples.

Increase of Si/Al ratio of samples resulted in an increase of the intensity of the resonance at −112 ppm [Si(4Si) species] and the decrease of the intensity of shoulder in the range of −90. 2 ppm to −99 ppm [AlOSi*(OSi)$_3$] species indicating a decrease in the number of Al framework species (Table 2). Combining the ^{27}Al and ^{29}Si MAS NMR spectral results, it is clear that the synthesized samples possessed both MFI and amorphous silica phases and increase of Si/Al ratio resulted in the formation of Si(4Si) sites and extra-framework Al species. The MAS NMR results clearly indicate that Si/Al ratio has an influence on the coordination of Al and Si atoms, which could subsequently affect the acidic properties of the samples.

Table 2. Types of Aluminum and total number of acid sites for studied samples.

| Sample	% Al_{FAl}^{IV} Atoms [a]	% Al_{EFAl}^{IV} Atoms [b]	Total Number of Acid Sites (mmoL g^{-1}) [c]
MFI-40	90.44	9.56	0.25
MFI-45	78.20	21.80	0.28
MFI-50	67.34	32.34	0.16
Zeolyst	95.13	4.87	0.39

[a, b] Framework (*FAl*) and non-framework (*EFAl*) of Al atoms are estimated from ^{29}Si MAS NMR; [c] number of acid sites estimated from NH$_3$-TPD analysis.

2.2. Acidity Measurments

The NH$_3$ desorption temperature is directly indicative of a strength of acid sites presented in the samples [48]. The synthesized H-ZSM-5 samples exhibited different NH$_3$-TPD profiles compared to the Zeolyst sample (Figure S2). Two major NH$_3$ desorption peaks were observed for the Zeolyst sample with maxima at 175 °C and 370 °C indicating the presence of weak and strong acid sites, respectively.

A decrease of the total acidity of the synthesized zeolite samples as measured by a lower amount of NH$_3$ desorbed (Figure S2 and Table 2), indicating the decrease in number and strength of the acid sites in the synthesized samples compared to the Zeolyst sample. Furthermore, we studied the acidic properties of samples by using CO as a probe molecule; it is known that CO has several advantages as a probe molecule such as weak basicity, small diameter, and high sensitivity to IR frequency [49]. Figure 6 shows FT-IR spectra of all the investigated samples after CO adsorption. The spectra were divided into two regions—spectra in the range of 3800–3100 cm^{-1} (a) and in the range of 2250–2100 cm^{-1} (b).

The FT-IR spectra presented in red correspond to the samples treated at 300 °C under vacuum. The upper spectra in blue are related to the highest CO pressure and the grey spectra in between are the set of spectra recorded with increase of CO pressure. For the Zeolyst sample, the intensity of the band at 3612 cm^{-1} corresponding to Si-OH-Al species (Brønsted acid sites) is clearly decreased with the increase of CO pressure. A new band clearly appeared at 3276 cm^{-1}, which could be attributed to CO coordinated to Si–OH–Al groups, Figure 6a. It can be seen that the intensity of the 3276 cm^{-1} band increased with an increase of CO pressure, indicating the higher strength of Brønsted acid sites in the Zeolyst sample. The intensity of the band at 3742 cm^{-1}, which is due to internal isolated Si–OH groups including a shoulder at 3722 cm^{-1}, decreased and another new band, due to formation of Si–OH–CO species, was clearly observed at 3641 cm^{-1}. Bleken et al. [22] reported very similar observations in the case of CO adsorbed on H-ZSM-5 nanosheet samples. The major difference between synthesized H-ZSM-5 samples and Zeolyst sample is that the synthesized samples exhibited a low-intensity band at 3612 cm^{-1}, which indicated that the synthesized samples possessed a lower density of Brønsted acid sites [38].
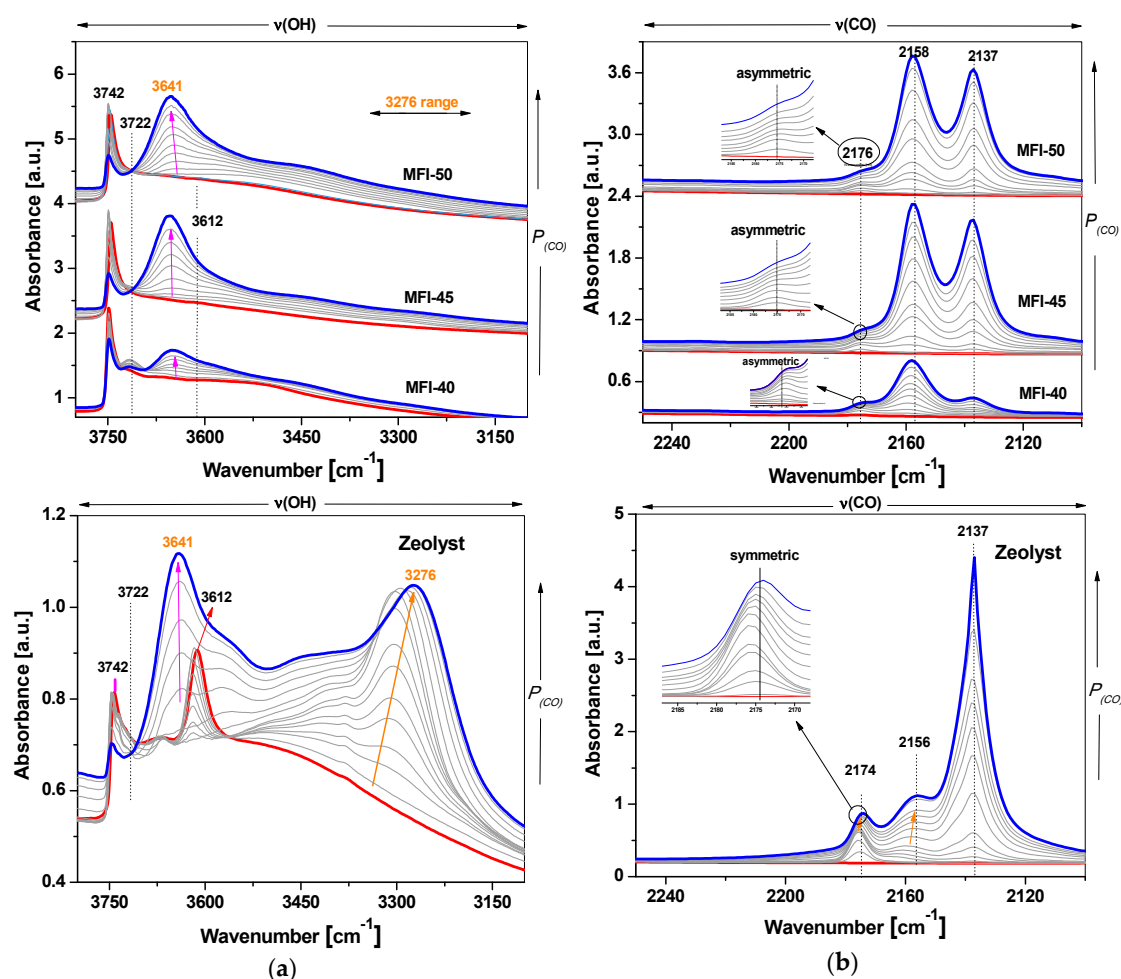

Figure 6. The FT-IR spectra after CO adsorption for synthesized H-ZSM-5 and Zeolyst samples; (**a**) in the range of 3800–3100 cm^{-1}, and (**b**) in the range of 2250–2100 cm^{-1}.

It was also reported that the IR absorption band at 2175 cm^{-1} could be due to CO interaction with Si-OH-Al groups [39]. This band was observed in the Zeolyst sample as well as in synthesized H-ZSM-5 samples. Leydier et al. [50] reported that amorphous silica-alumina materials showed the band at 2175 cm^{-1} with a tail, due to the adducts formed by -OH groups and framework Al sites on the external surfaces. Very similar FT-IR spectra were observed in the case of synthesized H-ZSM-5 samples. With the increase of CO pressure, the intensity of the band at 2175 cm^{-1} was also increased. From Figure 6b, we can notice that the most intense band was observed in the MFI-40 sample and the intensity decreased with the increase of Si/Al ratio. The band at 2175 cm^{-1} is sharp and symmetric in the case of the Zeolyst sample than the synthesized H-ZSM-5 samples. This is an indication of a homogeneous distribution of strong Brønsted acid sites in the Zeolyst sample, but not in the synthesized samples. Two additional bands appeared at 2158 cm^{-1} and 2137 cm^{-1} could be attributed to CO adsorbed on Si-OH species [51] and CO condensed in the pores of the zeolites [17,38,39], respectively. The band at 2137 cm^{-1} is sharp and intense in case of the Zeolyst sample, indicating that more CO molecules were trapped inside the micropores of the sample. However, synthesized H-ZSM-5 samples showed low peak areas under 2137 cm^{-1} peak compared to the Zeolyst sample (Figure S3 and Table S1), which is an indication that the synthesized samples possessed shortened channels with mesopores.

2.3. Catalytic Performance in the MTO Reaction

The catalytic performance of the samples was evaluated for the MTO reaction at 500 °C using a weight hourly space velocity (WHSV) of 3.0 h^{-1}. The methanol conversion and selectivity to different products for all the samples are presented in Figure 7.
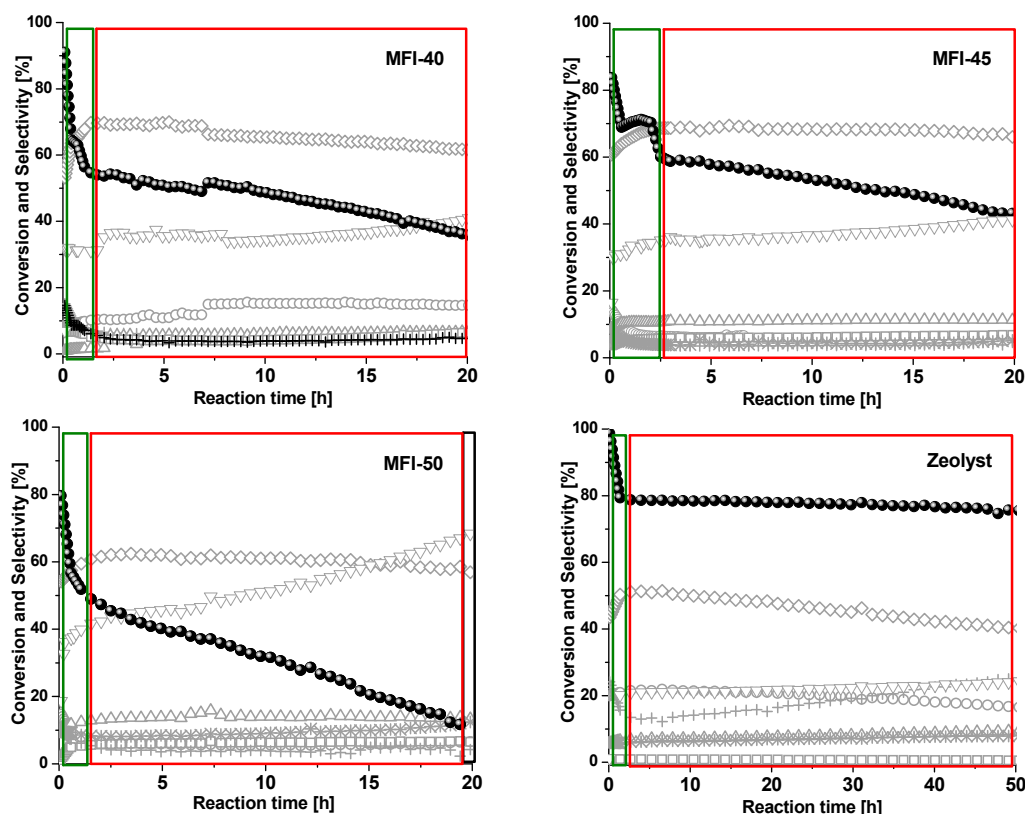

Figure 7. Methanol conversion and selectivity patterns of catalysts for the MTO reaction; reaction temperature: 500 °C and WHSV: 3 h^{-1}; (●) Methanol conversion, (○) C$_{2=}$, (◇) C$_{3=}$, (△) C$_{4=}$, (□) C$_{5=}$, (▽) DME, (*) paraffin, and (+) aromatics selectivity. The green region corresponds to the initial stage of reaction; where the products formation is initiated, the red region indicates to the stable/slower deactivation; where the products formation reaches to steady state, and the black region relates to the deactivated stage, where the products formation decreased drastically (below 20%).

After a short induction period, the Zeolyst sample offered 80% conversion at 500 °C. Synthesized H-ZSM-5 samples offered lower methanol conversions (maximum 72%) and low stability. Among the synthesized samples, MFI-45 exhibited better stability compared to MFI-40 and MFI-50 catalysts. The drastic decrease of methanol conversion at the initial stage could be related to accumulation of non-active hydrocarbon species in the pores of ZSM-5 structure [52,53]. The selectivity to propylene ($C_{3=}$), for all synthesized H-ZSM-5 samples is higher compared to Zeolyst sample. At the initial stage of reaction, the synthesized H-ZSM-5 samples showed different selectivity values; MFI-40 and MFI-50 samples offered 54%, while MFI-45 sample offered 60.7%, respectively. On the other hand, the Zeolyst sample offered only 43.5%. However, the selectivity towards ethylene ($C_{2=}$), is higher in the case of the Zeolyst sample compared to all synthesized H-ZSM-5 samples as shown in Figure 7. The Zeolyst sample showed $C_{2=}$ selectivity of about ~20%, while all synthesized H-ZSM-5 samples offered below 10%; therefore, synthesized H-ZSM-5 samples are more selective towards propylene formation.

The synthesized H-ZSM-5 samples showed higher propylene/ethylene ($C_{3=}/C_{2=}$) ratio in comparison to the Zeolyst sample (Figure S4). Propylene selectivity of all synthesized H-ZSM-5 samples remain stable in a steady state for 22 h and start to decrease with further increase of reaction time. Among the three samples, the MFI-45 sample showed higher and stable propylene selectivity. There are some other products, such as $C_{4=}$, $C_{5=}$, paraffins and aromatics, and their selectivity remains stable (lower than 15%). The Zeolyst sample exhibited slightly higher selectivity for $C_{4=}$, $C_{5=}$, aromatics and paraffins. This is most probably due to the fact that the Zeolyst sample possessed relatively high strong acid sites, which favors hydride transfer reactions to form C_1-C_5, paraffins, and aromatics [54,55]. Operando UV-vis spectroscopy is a very useful tool to detect the formation of carbonaceous species within the catalysts during the MTO reaction. When methanol passes through the catalyst bed, UV-vis spectra were collected for every 20 s (Figure S5). The growing of the UV-vis bands is an indication for the formation of hydrocarbon pool (HCP) species within the H-ZSM-5 structure. It was reported that the MTO reaction is an indirect reaction and the reaction pathway involved the formation of a methoxy species, protonated dimethyl ether, and water [56], followed by formation of HCP species to obtain aromatics and higher alkenes [57,58].

Due to the complexity and broadness of operando UV-vis spectra, a non-negative matrix factorization (NNMF) analysis was applied to obtain a better insight of different intermediate HCP species and their kinetic behavior [57]. The NNMF analysis of operando UV-vis spectra was divided into two groups—UV-vis Eigen spectra, and kinetic behavior of the HCP species. Figure 8 represents UV-vis Eigen spectra of different HCP species formed within ZSM-5 structure. The Zeolyst sample exhibited two major absorption bands of active species at 590 nm and 747 nm, which could be assigned to phenanthrene/anthracene carbocation and pyrenes species, respectively [57]. Meanwhile, synthesized H-ZSM-5 samples showed major absorption bands at 450 nm, 575 nm, and 710 nm corresponding to methylated naphthalene carbocations, phenanthrene/anthracene carbocation, and pyrenes, respectively. All the catalyst samples exhibiting broad bands correspond to deactivated species (poly-methylated and poly-cyclic aromatic species) [57].

The evolution of intermediate species as a function of reaction time is presented in Figure 9. It is clear that the formation of active HCP and coke species are initiated at different reaction times. The Zeolyst and MFI-40 samples require around ~0.1 h to initiate the HCP species, while MFI-45 and MFI-50 samples initiated these species at 0.14 and 0.18 h, respectively (Table 3). It can be observed that the Zeolyst sample needs around 1.3 h to initiate the formation of the coke species. However, in the case of the MFI-40 sample, the coke species are initiated along with the HCP species at around 0.1 h; on the other hand, MFI-45 and MFI-50 catalysts required ~0.3 h to initiate the formation of coke species. The formation rate of the HCP species was calculated using the evolution of the active group at a specific time (~0.3 h) and is presented in Table 3. We observed that the MFI-45 sample exhibited high rate in growth of HCP species (showing average rate ~61 cg/h).
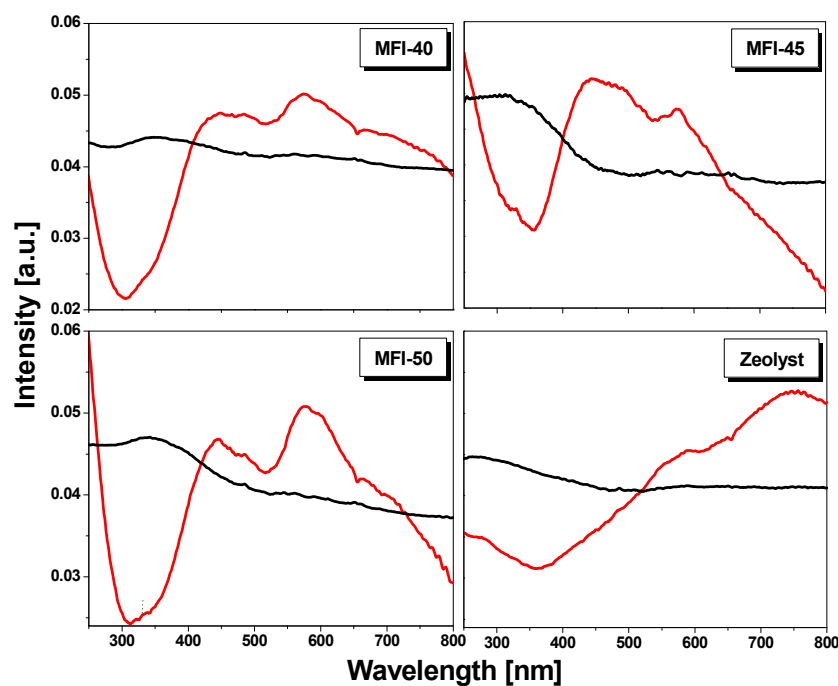
Figure 8. UV-vis Eigen spectra of investigated samples. Red colored spectra represent the active species, while black colored spectra represent the deactivated species, as determined by the NNMF method from operando UV-vis spectra.
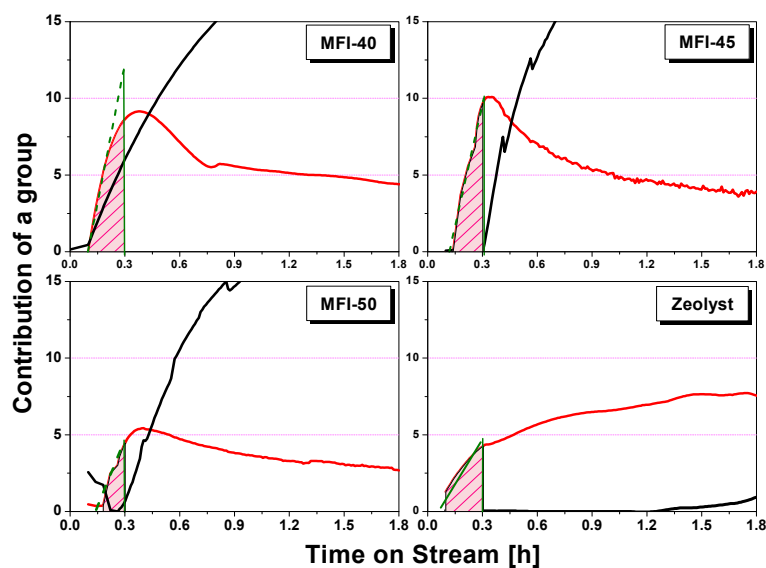
Figure 9. The evolution of intermediate species as a function of time; red represents the behavior of active species, while black represents the behavior of deactivated species.

Table 3. The average rate constant for the first formation of hydrocarbon pool and their initiation time [h].

Sample	Initiation Time for Active Species [h]	Initiation Time for Deactivating Species [h]	Average Rate for Growing of Active Species [cg/h^{-1}] [a]
MFI-40	0.10	0.1	45.5
MFI-45	0.14	0.3	61.5
MFI-50	0.18	0.3	37.0
Zeolyst	0.10	1.3	20.9

[a] cg/h: the contribution of active group per hour.

The dual-cycle concept is a widely accepted MTO mechanism for ZSM-5 materials, where ethylene is formed from an arene-based cycle, while propylene is formed from an olefin-based cycle [59] (Scheme S1) [60]. Therefore, the olefin distribution depends on which cycle is more dominant during the MTO reaction. It is well documented in the literature that the initiation of HCP species formation depends on the existence and the strength of Brønsted acid sites [61]. It was also observed that the generation of ethylene and formation of coke are dominant, if the catalyst possesses more strong Brønsted acid sites [54]. It was reported that both improved diffusion properties and lower acid strength are the reasons for observed high selectivity towards propylene in mesoporous ZSM-5 catalysts [62].

It is clear from the activity results that the active HCP species formation rate and the propylene selectivity are higher for all synthesized H-ZSM-5 samples, due to fact that these samples possessed low density of Brønsted acid sites. However, more Lewis acid sites (EFAl$^+$ species) were present in the synthesized samples compared to the Zeolyst sample. Corma et al. [14] and Mirodatos et al. [13] proposed that a synergistic effect exists between Brønsted and Lewis acid sites, and there is clear possibility that this synergistic effect played a role to obtain high rates of active HCP species formation in the case of synthesized H-ZSM-5 samples, especially in the MFI-45 sample. In addition, there is a limited hindrance from the structure in case of synthesized H-ZSM-5 samples. Therefore, the growth of HPC species was enhanced (from the intensity of bands of active HCP species). Presence of internal defect sites in synthesized samples is responsible for the formation of coke species along with the active HCP species at the beginning of the reaction. It was reported that the presence of internal defect sites enhances the accumulation of HCP species [38]. The propylene selectivity is higher at the beginning of the reaction in all the studied catalysts probably due to the fact that the intertwined alkene-arene-based cycle is dominant at this stage. By increasing the reaction time and more methanol exposure, the steady formation of propylene was observed in the case of synthesized H-ZSM-5 samples, which may be due to the domination of the alkene-based cycle. Consequently, the selectivity to other products for all synthesized H-ZSM-5 samples remains low in comparison with the Zeolyst sample. Therefore, we argue that the mechanism of the MTO reaction over synthesized H-ZSM-5 samples during the active stage is a cut-off dual-cycle process.

3. Experimental

3.1. Chemicals and Materials

The Si source, tetraethyl orthosilicate SiC$_8$H$_{20}$O$_4$ (>99%) and Al source, aluminum isopropoxide C$_9$H$_{21}$O$_3$Al (>96%) were purchased from Aldrich, UK. The template tetrapropyl ammonium hydroxide solution [(CH$_3$CH$_2$CH$_2$)$_4$N(OH)] (1.0 M in H$_2$O) was obtained from Sigma-Aldrich, while ammonium nitrate [(NH$_4$)NO$_3$, AR grade] for ion exchange was purchased from (Acros organics, Amsterdam, Netherlands Antilles). A commercial zeolite H-ZSM-5 (Si/Al = 40) catalyst material was provided by Zeolyst International. Methanol (99.9%) HPLC grade (Acros organics, Netherlands Antilles).

3.2. Catalyst Preparation

Synthesis of H-ZSM-5 Materials Embedded in Silica Matrix

ZSM-5 zeolites with different Si/Al ratios of 40, 45, and 50 were synthesized. The required amount of aluminum isopropoxide (0.5 g) was added to a 20 wt. % aqueous solution of 11 g tetrapropyl ammonium hydroxide (TPAOH). The mixture was placed in an ice bath under stirring to obtain a clear solution before adding the proper amount (20, 23, 26 ml for Si/Al ratios of 40, 45, and 50, respectively) of tetraethyl orthosilicate (TEOS). This mixture was stirred at room temperature for 24 h to hydrolyze TEOS completely. Thereafter, the solution was heated at 80 °C to remove water and alcohols. Finally, the obtained gel solution with 0.005 Al$_2$O$_3$:0.2 SiO$_2$:0.107 TPAOH:3.25 H$_2$O, 0.005 Al$_2$O$_3$:0.225 SiO$_2$:0.107 TPAOH:3.25 H$_2$O and 0.005 Al$_2$O$_3$:0.25 SiO$_2$:0.107 TPAOH:3.25 H$_2$O for the three synthesized samples of Si/Al ratio of 40, 45, and 50, respectively, was charged into a Teflon-lined stainless-steel autoclave and crystallized by thermal treatment under autogenous pressure

and static conditions at 120 °C for 16 h. After this treatment, the solid product was separated by centrifugation, washed several times with distilled water, dried overnight at 110 °C, and calcined in air at 550 °C for 6 h.

All synthesized ZSM-5 have been transformed into their protonic form, i.e., H-ZSM-5, by ion exchange with NH_4^+ ions and followed by calcination. The samples were heated before ion exchange procedure at 120 °C for 1 h. Then, the dried materials were added to 50 mL of 1.0 M NH_4NO_3 solution under continuous stirring. The samples were treated for 24 h at 60 °C. This step was repeated three times to achieve complete ion exchange. After completion of the ion exchange process, the samples were filtered using a polytetrafluoroethylene (PTFE) filter paper and washed with bi-distilled water. Finally, the obtained samples were calcined again in air at 550 °C for 6 h. The obtained samples were denoted as MFI-40, MFI-45, and MFI-50 with the number referring to the Si/Al ratios of 40, 45, and 50, respectively, of the materials under study. The commercial H-ZSM-5 sample from Zeolyst was also thermally treated at 550 °C for 6 h.

3.3. Characterization of Materials

The elemental composition of the zeolite materials under study was determined by inductively coupled plasma atomic emission spectroscopy (ICP-AES), Optima 7300DV, Perkin-Elmer Corporation, Waltham, MA, USA. Powder XRD studies were performed for all the prepared solid samples using a Bruker diffractometer (Bruker D8 advance target). The XRD patterns were obtained with a Co $K\alpha_{1,2}$ line and a monochromator ($\lambda = 1.79026$ Å) at 30 kV and 45 mA. The identification of different crystalline phases in the samples was performed by comparing the data with the Joint Committee for Powder Diffraction Standards (JCPDS) files. The lattice vibrations were measured by FT-IR spectroscopy in mid-range (400–4000 cm^{-1}), all the investigated samples were self-supported and not mixed with KBr. The morphology and particle size of the prepared ZSM-5 were investigated using a JEOL microscope and a model JSM-5600 SEM instrument. The textural properties of the prepared samples were determined from nitrogen adsorption/desorption measurements at −196 °C using ASiQ system (Quantachrome, Pleasanton, CA, USA). The specific surface area, S_{BET}, was calculated by applying the BET equation. The average pore radius was estimated from the relation $2V_{Total}/S_{BET}$, where V_{Total} is the total pore volume (at $P/P_0 = 0.975$). Pore-size distribution was generated by the NLDFT analysis of the adsorption branches, and the values for the average pore size were calculated. ^{27}Al and ^{29}Si MAS NMR spectra of the samples were obtained in single-pulse ("ZG") mode (3.5-ms pulses; 8-s delay between pulses) on a Bruker Avance 400 MHz spectrometer, operating at a frequency of 161.98 MHz. ^{29}Si chemical shifts were referenced to tetramethylsilane and the ^{27}Al chemical shifts were referenced to an aqueous solution of 0.5 M aluminum nitrate. The percentage of $Al^{IV}_{framework}$ and $Al^{VI}_{extra-framework}$ species were estimated from solid-state NMR spectral analysis and also by applying the formula; $(Si/Al)NMR = I/\sum 0.25n\, I_n$, where ($I$) represents the sum of the peak area of the NMR signals assigned to Si(nAl) building unit and (I_n) corresponds to the intensity of the resonance peak correspond to the $(AlO)_n Si(OSi)_{4-n}$ sites [63].

The acidic characteristic of the synthesized samples was determined by using NH_3-temperature-programmed desorption (NH_3-TPD) measurements performed on (Micrometric Autochem 2910 apparatus, Norcross, GA, USA). For the NH_3-TPD measurements, 100 mg of sample was crushed and sieved in a size of 212–425 μm. Subsequently, it was placed in a quartz tube reactor and packed with glass wool on both sides. The sample was preheated at 550 °C under helium gas flow (10 mL min^{-1}) for 15 min to remove any physiosorbed gases, and then the sample was saturated with NH_3 gas for 1 h at 100 °C. After that, the sample was flushed with helium gas for 1 h at 100 °C to remove any ammonia. Then, the desorption temperature increased from 100 to 600 °C under helium gas flow with a heating rate of 5 °C min^{-1} and NH_3-TPD patterns were collected by measuring the signal from a thermal conductivity detector (TCD). FT-IR spectra of the calcined catalysts obtained at room temperature using Perkin-Elmer Spectrum 100 FT-IR spectrometer. The CO adsorption FT-IR spectra collected in wavelength range of 4000–1000 cm^{-1} with 4 cm^{-1} resolution. For these experiments,

15–16 mg of catalyst sample was self-supported pressed into a pellet. The pellet was placed in the cryogenic cell (sample chamber), which was closed tightly. Then, the pellet was preheated from ambient temperature to 300 °C with rate of 5 °C min^{-1} and held for 1h under vacuum (6.9×10^{-6} mbar). Afterwards, the cell was cooled down to liquid nitrogen temperature (−196 °C) and first scan was collected before adsorption of CO start. The CO adsorption was carried out at −196 °C, start from 5.5×10^{-2} mbar till the pressure reach 10 mbar.

3.4. Catalytic MTO Reaction

All synthesized mesoporous H-ZSM-5 and the commercial Zeolyst H-ZSM-5 reference samples have been evaluated for the MTO reaction using an operando UV-vis spectroscopy reaction setup with online gas chromatography. Details of this setup can be found in recent literature [57]. Catalytic testing was done in a fixed-bed quartz reactor (4 cm in length, 0.1 mm thickness). The catalyst powder was pressed to give pellets, followed by crushing and sieving. The 212–425 μm fraction was used for catalytic testing. Prior to the reaction, ~50 mg of the catalyst was activated at 550 °C under the flow of 100% oxygen (10 mL h^{-1}) for 1 h and then cooled to the desired reaction temperature (500°C). The WHSV of methanol was kept at 3 h^{-1} by flowing helium gas through a methanol saturator. Analysis of the reactant and reaction products was performed with online gas chromatography (GC) by using an Interscience Compact GC instrument equipped with Rtx-1+Rtx-Wax, Rt-TCEP+Rtx-1 and Al$_2$O$_3$/Na$_2$SO$_4$ columns respectively and two flame ionization detectors (FIDs). The hydrocarbon pool intermediate species which generally forms during the MTO reaction was determined using an operando UV-vis absorption spectroscopy method. The measurements were performed in the wavelength range of 200–1800 nm using a high-temperature operando UV-vis probe manufactured by Avantes. The probe consists of one excitation and one collection fiber, which are connected to a Deuterium-Halogen light source and an Avaspec 2048 UV-vis spectroscope (Apeldoorn, NS, Netherlands).

4. Conclusions

H-ZSM-5 zeolites (Si/Al ratios of 40, 45, and 50) embedded in amorphous silica were successfully synthesized by a modified hydrothermal synthesis method. A set of characterization techniques were used to determine the structural, textural, and acidic properties of the synthesized materials. The synthesized H-ZSM-5 samples possessed the MFI structure, but exhibited lower Brønsted acid-site density and strength compared to a commercial microporous H-ZSM-5 sample. The variation of the Si/Al ratio affected the morphology, crystal size, and the porosity. The synthesized materials exhibited porosity comprising mesopores, thus showing substantially improved mass transport. The catalytic performance of the materials has been tested in the MTO process at 500 °C to understand the deactivation pattern of ZSM-5 catalysts. Interestingly, the synthesized materials offered high selectivity towards propylene (C$_{3=}$) in comparison with commercial Zeolyst sample under the same reaction conditions. The formation of hydrocarbon species during the MTO reaction has been studied with operando UV-vis spectroscopy in a fixed-bed reactor. The Zeolyst sample yielded phenanthrene/anthracene intermediate species, while the synthesized H-ZSM-5 samples majorly showed the presence of methylated naphthalene carbocations intermediate species. The synthesized H-ZSM-5 samples are favorable for forming active hydrocarbon species along with coke at the beginning of the reaction. The low density of Brønsted acid sites and the mesoporous nature of synthesized H-ZSM-5 catalysts are responsible for higher propylene selectivity.

reaction over (a) MFI-40; (b) MFI-45; (c) MFI-50 and (d) Zeolyst; WHSV: 3 h^{-1}, reaction temperature: 500 °C. The green colored spectra corresponds to the initial stage of reaction; where the products formation is initiated, the red colored spectra indicate to the stable/slower deactivation; where the products formation reach to the steady state, and the black colored spectra relates to the deactivated stage; where the products formation decreased drastically. Figure S6: The GC image for running MTO reaction of synthesized H-ZSM-5 (Si/Al = 50) sample. Scheme S1: The dual-cycle mechanistic concepts for conversion of methanol-to-olefins reaction over H-ZSM-5 catalysts. Table S1: Quantification data obtained from FT-IR spectra after CO adsorption (9.9 mbar pressure).

References

1. Mei, C.; Wen, P.; Liu, Z.; Liu, H.; Wang, Y.; Yang, W.; Xie, Z.; Hua, W.; Gao, Z. Selective production of propylene from methanol: Mesoporosity development in high silica HZSM-5. *J. Catal.* **2008**, *258*, 243–249. [CrossRef]

2. Corma, A.; Mengual, J.; Miguel, P. IM-5 zeolite for steam catalytic cracking of naptha to produce propene and ethane. An alternative to ZSM-5 zeolite. *J. Appl. Catal. A Gen.* **2013**, *460–461*, 106–115. [CrossRef]

3. Meng, T.; Mao, D.; Guo, Q.; Lu, G. The effect of crystal sizes of HZSM-5 zeolites in ethanol conversion to propylene. *Catal. Commun.* **2012**, *21*, 52–57. [CrossRef]

4. Yang, G.; Wei, Y.; Xu, S.; Chen, J.; Li, J.; Liu, Z.; Yu, J.; Xu, R. Nanosize-Enhaned Lifetime of SAPO-34 Catalysts in Methanol-to-Olefin Reaction. *J. Phys. Chem. C* **2013**, *117*, 8214–8222. [CrossRef]

5. Jo, C.; Jung, J.; Shin, H.S.; Kim, J.; Ryoo, R. Capping with Multivalent Surfactants for Zeolite Nanocrystal Synthesis. *Angew. Chem. Int. Ed.* **2013**, *52*, 10014–10017. [CrossRef]

6. Tian, P.; Wei, Y.; Ye, M.; Liu, Z. Methanol to Olefins (MTO): From Fundamentals to Commercialization. *ACS Catal.* **2015**, *5*, 1922–1938. [CrossRef]

7. Hong, Y.; Gruver, V.; Fripiat, J.J. Role of Lewis Acidity in the Isomerization of n-Pentane and o-Xylene on Dealuminated H-Mordenites. *J. Catal.* **1994**, *150*, 421–429. [CrossRef]

8. Goetze, J.; Meirer, F.; Yarulina, I.; Gascon, J.; Kapteijn, F.; Ruiz-Martínez, J.; Weckhuysen, B.M. Insights into the Activity and Deactivation of the Methanol-to-Olefins Process over Different Small-Pore Zeolites As Studied with Operando UV–vis Spectroscopy. *ACS Catal.* **2017**, *7*, 4033–4046. [CrossRef]

9. Catizzone, E.; Cirelli, Z.; Aloise, A.; Lanzafame, P.; Migliori, M.; Giordano, G. Methanol conversion over ZSM-12, ZSM-22 and EU-1 zeolites: From DME to hydrocarbons production. *Catal. Today* **2018**, *304*, 39–50. [CrossRef]

10. Palčić, A.; Ordomsky, V.V.; Qin, Z.; Georgieva, V.; Valtchev, V. Tuning Zeolite Properties for a Highly Efficient Synthesis of Propylene from Methanol. *Chem. Eur. J.* **2018**, *24*, 13136–13149. [CrossRef]

11. Losch, P.; Boltz, M.; Bernardon, C.; Louis, B.; Palčić, A.; Valtchev, V. Impact of external surface passivation of nano-ZSM-5 zeolites in the methanol-to-olefins reaction. *Appl. Catal. A Gen.* **2016**, *509*, 30–37. [CrossRef]

12. Ibáñez, M.; Epelde, E.; Aguayo, A.T.; Gayubo, A.G.; Bilbao, J.; Castaño, P. Selective dealumination of HZSM-5 zeolite boosts propylene by modifying 1-butene cracking pathway. *Appl. Catal. A Gen.* **2017**, *543*, 1–9. [CrossRef]

13. Mirodatos, C.; Barthomeuf, D. Superacid sites in zeolites. *J. Chem. Soc. Chem. Commun.* **1981**, 39–40. [CrossRef]

14. Corma, A.; Fornés, V.; Rey, F. Extraction of extra-framework aluminium in ultrastable Y zeolites by (NH$_4$)2SiF$_6$ treatments: I. Physicochemical Characterization. *Appl. Catal.* **1990**, *59*, 267–274. [CrossRef]

15. Däumer, D.; Räuchle, K.; Reschetilowski, W. Experimental and Computational Investigations of the Deactivation of H-ZSM-5 Zeolite by Coking in the Conversion of Ethanol into Hydrocarbons. *ChemCatChem* **2012**, *4*, 802–814. [CrossRef]

16. Hadi, N.; Niaei, A.; Nabavi, S.R.; Farzi, A.; Shirazia, M.N. Development of a New Kinetic Model for Methanol to Propylene Process on Mn/H-ZSM-5 Catalyst. *Chem. Biochem. Eng. Q.* **2014**, *28*, 53.

17. Bleken, F.L.; Chavan, S.; Olsbye, U.; Boltz, M.; Ocampo, F.; Louis, B. Conversion of methanol into light olefins over ZSM-5 zeolite: Strategy to enhance propene selectivity. *Appl. Catal. A Gen.* **2012**, *447–448*, 178–185. [CrossRef]

18. Xi, D.; Sun, Q.; Xu, J.; Cho, M.; Cho, H.S.; Asahina, S.; Li, Y.; Deng, F.; Terasaki, O.; Yu, J. In situ growth-etching approach to the preparation of hierarchically macroporous zeolites with high MTO catalytic activity and selectivity. *J. Mater. Chem. A* **2014**, *2*, 17994–18004. [CrossRef]

19. Perez-Ramirez, J.; Christensen, C.H.; Egeblad, K.; Christensen, C.H.; Groen, J.C. Hierarchical zeolites: Enhanced utilisation of microporous crystals in catalysis by advances in materials design. *Chem. Soc. Rev.* **2008**, *37*, 2530–2542. [CrossRef]

20. Li, L.; Cui, X.; Li, J.; Wang, J. Synthesis of SAPO-34/ZSM-5 Composite and Its Catalytic Performance in the Conversion of Methanol to Hydrocarbonsc. *J. Braz. Chem. Soc.* **2014**, *26*, 290–296. [CrossRef]

21. Conte, M.; Xu, B.; Davies, T.E.; Bartley, J.K.; Carley, A.F.; Taylor, S.H.; Khalid, K.; Hutchings, G.J. Enhanced selectivity to propene in the methanol to hydrocarbons reaction by use of ZSM-5/11 intergrowth zeolite. *Microporous Mesoporous Mater.* **2012**, *164*, 207–213. [CrossRef]

22. Lonstad Bleken, B.-T.; Mino, L.; Giordanino, F.; Beato, P.; Svelle, S.; Lillerud, K.P.; Bordiga, S. Probing the surface of nanosheet H-ZSM-5 with FTIR spectroscopy. *Phys. Chem. Chem. Phys.* **2013**, *15*, 13363–13370. [CrossRef] [PubMed]

23. Müller, S.; Liu, Y.; Vishnuvarthan, M.; Sun, X.; van Veen, A.C.; Haller, G.L.; Sanchez-Sanchez, M.; Lercher, J.A. Coke formation and deactivation pathways on H-ZSM-5 in the conversion of methanol to olefins. *J. Catal.* **2015**, *325*, 48–59. [CrossRef]

24. Zhang, S.; Gong, Y.; Zhang, L.; Liu, Y.; Dou, T.; Xu, J.; Deng, F. Hydrothermal treatment on ZSM-5 extrudates catalyst for methanol to propylene reaction: Finely tuning the acidic property. *Fuel Process. Technol.* **2015**, *129*, 130–138. [CrossRef]

25. Wu, W.; Guo, W.; Xiao, W.; Luo, M. Dominant reaction pathway for methanol conversion to propene over high silicon H-ZSM-5. *Chem. Eng. Sci.* **2011**, *66*, 4722–4732. [CrossRef]

26. Yarulina, I.; Bailleul, S.; Pustovarenko, A.; Martinez, J.R.; De Wispelaere, K.; Hajek, J.; Weckhuysen, B.M.; Houben, K.; Baldus, M.; Van Speybroeck, V.; et al. Suppression of the Aromatic Cycle in Methanol-to-Olefins Reaction over ZSM-5 by Post-Synthetic Modification Using Calcium. *ChemCatChem* **2016**, *8*, 3057–3063. [CrossRef]

27. Yarulina, I.; De Wispelaere, K.; Bailleul, S.; Goetze, J.; Radersma, M.; Abou-Hamad, E.; Vollmer, I.; Goesten, M.; Mezari, B.; Hensen, E.J.M.; et al. Structure–performance descriptors and the role of Lewis acidity in the methanol-to-propylene process. *Nat. Chem.* **2018**, *10*, 804–812.

28. Jacobs, P.A.; Derouane, E.G.; Weitkamp, J. Evidence for X-ray-amorphous zeolites. *Chem. Commun.* **1981**, 591–593. [CrossRef]

29. Nicolaides, C. A novel family of solid acid catalysts: Substantially amorphous or partially crystalline zeolitic materials. *Appl. Catal. A Gen.* **1999**, *185*, 211–217. [CrossRef]

30. Triantafyllidis, K.S.; Nalbandian, L.; Trikalitis, P.N.; Ladavos, A.K.; Mavromoustakos, T.; Nicolaides, C.P. Structural, compositional and acidic characteristics of nanosized amorphous or partially crystalline ZSM-5 zeolite-based materials. *Microporous Mesoporous Mater.* **2004**, *75*, 89–100. [CrossRef]

31. Corma, A.; Díaz-Cabañas, M.J. Amorphous microporous molecular sieves with different pore dimensions and topologies: Synthesis, characterization and catalytic activity. *Microporous Mesoporous Mater.* **2006**, *89*, 39–46. [CrossRef]

32. Tago, T.; Masuda, Y. Zeolite nanocrystals-synthesis and applications. In *Nanocrystals*; IntechOpen: London, UK, 2010; pp. 8–206.

33. Kim, W.J.; Kim, S.D. Method of Preparing zsm-5 Using Variable Temperature without Organic Template. U.S. Patent 7,361,328, 22 April 2008.

34. Yeong, Y.F.; Abdullah, A.Z.; Ahmad, A.L.; Bhatia, S. Propylsulfonic acid-functionalized partially crystalline silicalite-1 materials: Synthesis and characterization. *J. Porous Mater.* **2011**, *18*, 147–157. [CrossRef]

35. Mostafa, M.M.M.; Rao, K.N.; Harun, H.S.; Basahel, S.N.; El-Maksod, I.H.A. Synthesis and characterization of partially crystalline nanosized ZSM-5 zeolites. *Ceram. Int.* **2013**, *39*, 683–689. [CrossRef]
36. Haw, K.-G.; Gilson, J.-P.; Nesterenko, N.; Akouche, M.; El Siblani, H.; Goupil, J.-M.; Rigaud, B.; Minoux, D.; Dath, J.-P.; Valtchev, V. Supported Embryonic Zeolites and their Use to Process Bulky Molecules. *ACS Catal.* **2018**, *8*, 8199–8212. [CrossRef]
37. Cheng, Y.; Wang, L.-J.; Li, J.-S.; Yang, Y.-C.; Sun, X.-Y. Preparation and characterization of nanosized ZSM-5 zeolites in the absence of organic template. *Mater. Lett.* **2005**, *59*, 3427–3430. [CrossRef]
38. Barbera, K.; Bonino, F.; Bordiga, S.; Janssens, T.V.W.; Beato, P. Structure–deactivation relationship for ZSM-5 catalysts governed by framework defects. *J. Catal.* **2011**, *280*, 196–205. [CrossRef]
39. Bjørgen, M.; Svelle, S.; Joensen, F.; Nerlov, J.; Kolboe, S.; Bonino, F.; Palumbo, L.; Bordiga, S.; Olsbye, U. Conversion of methanol to hydrocarbons over zeolite H-ZSM-5: On the origin of the olefinic species. *J. Catal.* **2007**, *249*, 195–207. [CrossRef]
40. Robson, H.; Lillerud, K.P. *Verified Synthesis of Zeolitic Materials*; Elsevier: Amsterdam, The Netherlands, 2001.
41. Coster, D.; Blumenfeld, A.L.; Fripiat, J.J. Lewis Acid Sites and Surface Aluminum in Aluminas and Zeolites: A High-Resolution NMR Study. *J. Phys. Chem.* **1994**, *98*, 6201–6211. [CrossRef]
42. Corma, A.; Fornés, V.; Martínez, A.; Sanz, J. Tetrahedral and Octahedral Extraframework Aluminum in Ultrastable Y Zeolites. In *Fluid Catalytic Cracking*; American Chemical Society: Washington, DC, USA, 1988; pp. 2–17.
43. Kunkeler, P.J.; Zuurdeeg, B.J.; van der Waal, J.C.; van Bokhoven, J.A.; Koningsberger, D.C.; van Bekkum, H. Zeolite Beta: The Relationship between Calcination Procedure, Aluminum Configuration, and Lewis Acidity. *J. Catal.* **1998**, *180*, 234–244. [CrossRef]
44. Thomas, J.M.; Klinowski, J. The Study of Aluminosilicate and Related Catalysts by High-Resolution Solid-State NMR Spectroscopy. *Adv. Catal.* **1985**, *33*, 199–374.
45. Fyfe, C.A.; Gobbi, G.C.; Kennedy, G.J.; Graham, J.D.; Ozubko, R.S.; Murphy, W.J.; Bothner-By, A.; Dadok, J.; Chesnick, A.S. Detailed interpretation of the 29Si and 27Al high-field MAS n.m.r. spectra of zeolites offretite and omega. *Zeolites* **1985**, *5*, 179–183. [CrossRef]
46. Zhu, L.; Yin, S.; Wang, X.; Liu, Y.; Wang, S. The catalytic properties evolution of HZSM-5 in the conversion of methanol to gasoline. *RSC Adv.* **2016**, *6*, 82515–82522. [CrossRef]
47. Jacobsen, C.J.H.; Madsen, C.; Janssens, T.V.W.; Jakobsen, H.J.; Skibsted, J. Zeolites by confined space synthesis—Characterization of the acid sites in nanosized ZSM-5 by ammonia desorption and ^{27}Al/29Si-MAS NMR spectroscopy. *Microporous Mesoporous Mater.* **2000**, *39*, 393–401. [CrossRef]
48. Costa, C.; Dzikh, I.P.; Lopes, J.M.; Lemos, F.; Ribeiro, F.R. Activity–acidity relationship in zeolite ZSM-5. Application of Brönsted-type equations. *J. Mol. Catal. A Chem.* **2000**, *154*, 193–201. [CrossRef]
49. Kondo, J.N.; Nishitani, R.; Yoda, E.; Yokoi, T.; Tatsumi, T.; Domen, K. A comparative IR characterization of acidic sites on HY zeolite by pyridine and CO probes with silica-alumina and [gamma]-alumina references. *Phys. Chem. Chem. Phys.* **2010**, *12*, 11576–11586. [CrossRef] [PubMed]
50. Leydier, F.; Chizallet, C.; Costa, D.; Raybaud, P. CO adsorption on amorphous silica-alumina: Electrostatic or Bronsted acidity probe? *Chem. Commun.* **2012**, *48*, 4076–4078. [CrossRef] [PubMed]
51. Hattori, H.; Ono, Y. *Solid Acid Catalysis: From Fundamentals to Applications*; Tylor & Francis Group: Boca Raton, FL, USA, 2015.
52. Tanabe, K.; Misono, M.; Ono, Y.; Hattori, H. *New Solid Acids and Bases: Their Catalytic Properties (Studies in Surface Science and Catalysis)*; Elsevier Science Ltd.: Amsterdam, The Netherlands, 1989.
53. Moreno-Piraján, J.C.; Garcia-Cuello, V.S.; Giraldo, L. Synthesis of HMOR and HZSM-5 and their Behaviour in the Catalytic Conversion of Methanol to Propylene (MTP). *J. Thermodyn. Catal.* **2010**, *1*, 101. [CrossRef]
54. Lin, L.; Qiu, C.; Zhuo, Z.; Zhang, D.; Zhao, S.; Wu, H.; Liu, Y.; He, M. Acid strength controlled reaction pathways for the catalytic cracking of 1-butene to propene over ZSM-5. *J. Catal.* **2014**, *309*, 136–145. [CrossRef]
55. Castaño, P.; Gayubo, A.G.; Pawelec, B.; Fierro, J.L.G.; Arandes, J.M. Kinetic modelling of methylcyclohexane ring-opening over a HZSM-5 zeolite catalyst. *Chem. Eng. J.* **2008**, *140*, 287–295. [CrossRef]
56. Qian, Q.; Vogt, C.; Mokhtar, M.; Asiri, A.M.; Al-Thabaiti, S.A.; Basahel, S.N.; Ruiz-Martínez, J.; Weckhuysen, B.M. Combined Operando UV/Vis/IR Spectroscopy Reveals the Role of Methoxy and Aromatic Species during the Methanol-to-Olefins Reaction over H-SAPO-34. *ChemCatChem* **2014**, *6*, 3396–3408. [CrossRef]

57. Borodina, E.; Meirer, F.; Lezcano-González, I.; Mokhtar, M.; Asiri, A.M.; Al-Thabaiti, S.A.; Basahel, S.N.; Ruiz-Martinez, J.; Weckhuysen, B.M. Influence of the reaction temperature on the nature of the active and deactivating species during methanol to olefins conversion over H-SSZ-13. *ACS Catal.* **2015**, *5*, 992–1003. [CrossRef]

58. Borodina, E.; Kamaluddin, H.S.H.; Meirer, F.; Mokhtar, M.; Asiri, A.M.; Al-Thabaiti, S.A.; Basahel, S.N.; Ruiz-Martinez, J.; Weckhuysen, B.M. Influence of the Reaction Temperature on the Nature of the Active and Deactivating Species During Methanol-to-Olefins Conversion over H-SAPO-34. *ACS Catal.* **2017**, *7*, 5268–5281. [CrossRef]

59. Sun, X.; Mueller, S.; Shi, H.; Haller, G.L.; Sanchez-Sanchez, M.; van Veen, A.C.; Lercher, J.A. On the impact of co-feeding aromatics and olefins for the methanol-to-olefins reaction on HZSM-5. *J. Catal.* **2014**, *314*, 21–31. [CrossRef]

60. Bjørgen, M.; Joensen, F.; Lillerud, K.-P.; Olsbye, U.; Svelle, S. The mechanisms of ethene and propene formation from methanol over high silica H-ZSM-5 and H-beta. *Catal. Today* **2009**, *142*, 90–97. [CrossRef]

61. Campbell, S.M.; Jiang, X.-Z.; Howe, R.F. Methanol to hydrocarbons: Spectroscopic studies and the significance of extra-framework aluminium. *Microporous Mesoporous Mater.* **1999**, *29*, 91–108. [CrossRef]

62. Westgård Erichsen, M.; De Wispelaere, K.; Hemelsoet, K.; Moors, S.L.C.; Deconinck, T.; Waroquier, M.; Svelle, S.; Van Speybroeck, V.; Olsbye, U. How zeolitic acid strength and composition alter the reactivity of alkenes and aromatics towards methanol. *J. Catal.* **2015**, *328*, 186–196. [CrossRef]

63. Song, C.; Wang, M.; Zhao, L.; Xue, N.; Peng, L.; Guo, X.; Ding, W.; Yang, W.; Xie, Z. Synergism between the Lewis and Brönsted acid sites on HZSM-5 zeolites in the conversion of methylcyclohexane. *Chin. J. Catal.* **2013**, *34*, 2153–2159. [CrossRef]